Meteorol. Atmos. Phys. 65, 11–30 (1998)

Meteorology and Atmospheric Physics

[1] Istituto FISBAT-CNR, Bologna, Italy
[2] Istituto ISIATA-CNR, Lecce, Italy

Relative Optical Mass Functions for Air, Water Vapour, Ozone and Nitrogen Dioxide in Atmospheric Models Presenting Different Latitudinal and Seasonal Conditions

C. Tomasi[1], **V. Vitale**[1], and **L. V. De Santis**[2]

With 9 Figures

Received April 18, 1997
Revised September 30, 1997

Summary

A study of the dependence features of the relative optical mass functions for air, water vapour, ozone and nitrogen dioxide on the apparent solar zenith angle θ was performed by calculating these optical parameters by means of the well-known computer code LOWTRAN 7 at several values of θ and for nine atmospheric models characterized by different latitudes and seasons. Moreover, other investigations were performed on the dependence features of (i) the relative optical air mass on the thermal characteristics of the low troposphere, (ii) the relative optical water vapour mass on the vertical distribution characteristics of absolute humidity in the troposphere, and (iii) the relative optical mass function for ozone and nitrogen dioxide on the shape characteristics of the vertical profiles of the two gaseous concentrations and the concentration peak altitudes. The results are compared with the values given by the two simple formulas proposed by Kasten (1966) for air and water vapour and the formulas defined by Young (1969) and Staehelin et al. (1995) for ozone and nitrogen dioxide. From this comparison, a wide set of correction factors were obtained which can be conveniently used in the analysis of multispectral sun-radiometric measurements for calculating, with a very high precision, the values of the four optical mass functions at all the angles θ in the 0° to 87° range, corresponding to the various latitudinal and seasonal conditions described by the nine atmospheric models.

1. Introduction

The solar radiation reaching the terrestrial surface is strongly attenuated by scattering and absorption phenomena taking place in the atmosphere. As a consequence of these interactions, only a limited percentage of the incoming extraterrestrial solar irradiance directly reaches the earth's surface, while another important fraction arrives at the ground in the form of diffuse radiation produced largely by Rayleigh scattering and to a variable extent by aerosol particles. Another significant percentage is back-scattered by the atmosphere toward the space, while the remaining part is absorbed by aerosol particles and various atmospheric gases. The percentages of solar radiation subject to atmospheric scattering and absorption can be correctly evaluated from ground-based measurements taken with spectroradiometers (Dobson, 1931; Brewer, 1973; Volz, 1974; Kulkarni, 1975; Nakajima et al., 1996). In particular, precise measurements of direct solar irradiance can be taken using multiwavelength sun-photometers characterized by narrow widths of the field of view (Shaw, 1976; Tomasi et al., 1983). From these measurements, reliable evaluations of atmospheric transmission along the sun-path can be obtained at various wavelengths in the visible and near-infrared spectral range and for different solar zenith angles. From each monochromatic measurement of transmitted solar irradiance, the product of the

total atmospheric optical depth by the effective air mass can be evaluated. This quantity can be represented as the sum of partial terms due to Rayleigh scattering, aerosol extinction and gaseous absorption produced mainly by water vapour, ozone and nitrogen dioxide (Thomason et al., 1983). Each partial term is given by the product of two physical parameters: (i) the optical depth produced by a single atmospheric constituent, and (ii) the corresponding relative optical mass, given by the ratio of the optical path along the oblique trajectory followed by the solar photons to the optical path in the zenith direction (Kasten, 1966; Iqbal, 1983).

The monochromatic optical depth of each atmospheric constituent is substantially given by the integral of the volume absorption coefficient along the vertical path. This parameter is mainly related to the total mass of the atmospheric constituent in the vertical atmospheric column of unit cross section and only weakly depends on the shape of the vertical distribution curve of the extinction coefficient. The relative optical air mass function depends mainly on the geometrical length of the sun-path and, thus, on the solar zenith angle, although it can also be appreciably influenced by the vertical distribution characteristics of air density and, consequently, on the vertical temperature profile (Penndorf, 1957). Therefore, the relative optical air mass can vary appreciably for high values of the solar zenith angle as a function of the thermal characteristics of the atmosphere and, thus, with latitude and season. Similarly, the relative optical mass functions for minor atmospheric gases depend on the solar zenith angle through features related to the vertical distribution curves of the atmospheric gases. All aspects concerning the variability of the relative optical mass for air, water vapour, ozone and nitrogen dioxide due to changes in the atmospheric conditions depending on the latitude and season are examined in the present paper by means of simulation studies; the results are compared with the values of the relative optical mass given by the formulas most commonly used in the literature (Kasten, 1966; Young, 1969).

However, before describing the procedures adopted to perform the relevant calculations, it is useful to define the concepts of the physical parameters and briefly describe the formulas proposed by Kasten (1966) and Young (1969), which are commonly used to determine the dependence features of the four air mass functions on the zenith angle of the sun.

2. The Relative Optical Mass for Air and some Gaseous Constituents of the Atmosphere

When a parallel beam of monochromatic radiation traverses an atmospheric layer containing air molecules only, each volume element of the atmosphere extinguishes the incoming radiation beam in a measure closely related to the number concentration of the air molecules. Thus, the total atmospheric mass distributed along the oblique trajectory described by the incoming beam is given by the integral of total air density along the whole trajectory, from the ground-level to the top-level of the atmosphere, that is

$$m = \int_0^\infty \rho \, \mathrm{d}s, \tag{1}$$

where ρ is the density of the atmospheric medium and $\mathrm{d}s$ is the element of the geometrical path length described by the solar direct radiation beam. The latter quantity is dependent on the refractive index of air and, consequently, on wavelength. In the extreme case where the solar radiation incomes vertically, the geometrical path length $\mathrm{d}s$ coincides with the infinitesimal element $\mathrm{d}z$ taken along the vertical path, so that the optical mass in the vertical direction is given by the integral m_z of air density calculated along the vertical path of the atmosphere. Parameter m_z gives a measure of the total mass of the substance producing extinction in the vertical atmospheric column of unit cross section. Consequently, this parameter is independent on the refractive index and, hence, on wavelength. The relative optical mass m_r pertinent to a certain atmospheric constituent can be evaluated as the ratio m/m_z and gives a measure of the optical mass distributed along the oblique trajectory and normalized to the vertical path.

On the basis of these general concepts, the relative optical mass functions for dry air, water vapour, ozone and nitrogen dioxide are usually calculated as a function of the solar zenith angle by means of different approximation formulas, as follows.

2.1 Kasten's Formula giving the Relative Optical Mass for Dry Air

Taking into account both the earth's curvature and atmospheric refraction, Kasten (1966) defined the relative optical air mass m_a for dry air in terms of the following equation,

$$m_a(\theta) = \int_0^\infty \left\{1 - \left[1 + 2(1+n_o)\left(1 - \frac{\rho(z)}{\rho_o}\right)\right] \times \left(\frac{R}{R+z}\right)^2 \sin^2\theta\right\}^{-0.5} \rho(z)\mathrm{d}z \Big/ \int_0^\infty \rho(z)\mathrm{d}z \quad (2)$$

where:

- n_o is the refractive index of air at ground-level;
- $\rho(z)$ is the air density at height z;
- ρ_o is the air density at ground-level;
- R is the mean radius of the earth, equal to 6371.229 km; and
- θ is the apparent solar zenith angle of the sun, as defined by the scheme shown in Fig. 1.

Equation (2) was applied by Kasten (1966) to the vertical profile of air density, as given by the ARDC (Air Research and Development Command) Model Atmosphere, 1959 (Minzner et al., 1959) from the sea-level to the height of 84 km, in which the ground-level temperature was taken as equal to 15 °C, the ground-level air pressure to 1013.25 hPa, the ground-level air density to 1.225 10^{-3} g cm^{-3} and the air refractive index n_o to 1.000276. The integral in Eq. (2) was calculated by Kasten (1966) for a limited number of selected values of θ by dividing the atmosphere into a great number of homogeneous sublayers with depths of 0.1 km from the sea-level to the height $z = 19.6$ km, 0.2 km from here to a height of 50 km and 0.5 km from 50 km to the top-level of 84 km.

Following this procedure, Kasten (1966) found a best-fit solution given by the following equation

$$m_a(\theta) = [\cos\theta + 0.15(93.885 - \theta)^{-1.253}]^{-1}, \quad (3)$$

which defines the dependence curve of m_a on θ shown in Fig. 2. The values of $m_a(\theta)$ found for thirty values of θ from 0° to 87° are given in Table 1. The results show that the value of $m_a(\theta)$

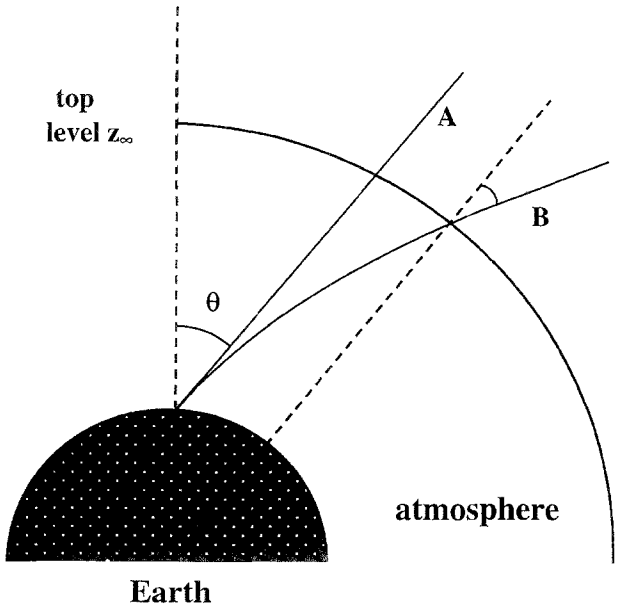

Fig. 1. Model of the earth's atmosphere showing that the apparent solar zenith angle θ is the angle of the nonrefracted solar ray A with the local normal at sea-level (that is, the angle under which the Sun is "seen" by the observer at the earth's surface). The refracted solar ray is labeled with B

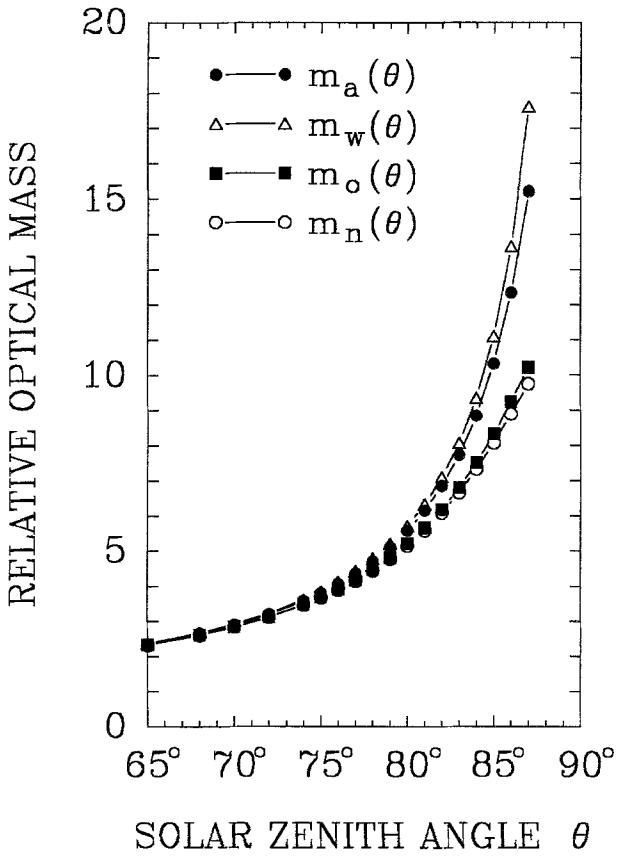

Fig. 2. Relative optical mass functions $m_a(\theta)$ for air, $m_w(\theta)$ for water vapour, $m_o(\theta)$ for ozone and $m_n(\theta)$ for nitrogen dioxide plotted versus the apparent solar zenith angle θ in the range from 65° to 87°

Table 1. *Values of Relative Optical Air Mass $m_a(\theta)$ Calculated Using the Kasten Formula given in Eq. (4), Relative Optical Air Mass $\mu_a(\theta)$ Calculated by Kasten and Young (1989), Ratio $\Gamma(\theta) = \mu_a(\theta)/m_a(\theta)$, Relative Optical Air Mass $m_w(\theta)$ given by Eq. (5), Relative Optical Mass $m_o(\theta)$ given by Eq. (6) for $h = h_o = 22$ km and Relative Optical Mass $m_n(\theta)$ given by Eq. (6) for $h = h_n = 25$ km, all Pertinent to thirty Values of the Apparent Solar Zenith angle θ*

$\theta(^\circ)$	$m_a(\theta)$	$\mu_a(\theta)$	$\Gamma(\theta)$	$m_w(\theta)$	$m_o(\theta)$	$m_n(\theta)$
0	0.9995	1.0000	1.0005	0.9999	1.0000	1.0000
10	1.0148	1.0154	1.0006	1.0153	1.0153	1.0153
15	1.0346	1.0352	1.0006	1.0352	1.0350	1.0350
20	1.0634	1.0640	1.0006	1.0641	1.0637	1.0636
25	1.1025	1.1031	1.0005	1.1032	1.1026	1.1024
30	1.1536	1.1543	1.0006	1.1545	1.1534	1.1532
35	1.2194	1.2202	1.0007	1.2205	1.2187	1.2184
40	1.3037	1.3045	1.0006	1.3051	1.3023	1.3018
45	1.4119	1.4128	1.0006	1.4138	1.4094	1.4087
50	1.5526	1.5535	1.0006	1.5552	1.5482	1.5472
55	1.7388	1.7398	1.0006	1.7426	1.7314	1.7297
60	1.9928	1.9939	1.0006	1.9986	1.9797	1.9770
65	2.3539	2.3552	1.0006	2.3637	2.3297	2.3249
68	2.6515	2.6529	1.0005	2.6658	2.6150	2.6079
70	2.8999	2.9016	1.0006	2.9188	2.8508	2.8413
72	3.2035	3.2054	1.0006	3.2290	3.1356	3.1227
74	3.5819	3.5841	1.0006	3.6177	3.4853	3.4672
75	3.8081	3.8105	1.0006	3.8511	3.6911	3.6695
76	4.0656	4.0682	1.0006	4.1179	3.9225	3.8963
77	4.3612	4.3640	1.0006	4.4255	4.1839	4.1519
78	4.7036	4.7067	1.0007	4.7842	4.4811	4.4415
79	5.1047	5.1081	1.0007	5.2072	4.8208	4.7713
80	5.5803	5.5841	1.0007	5.7135	5.2117	5.1489
81	6.1526	6.1565	1.0006	6.3297	5.6637	5.5830
82	6.8531	6.8568	1.0005	7.0952	6.1891	6.0836
83	7.7279	7.7307	1.0004	8.0705	6.8009	6.6610
84	8.8474	8.8475	1.0000	9.3530	7.5119	7.3239
85	10.3231	10.3164	0.9994	11.1097	8.3292	8.0743
86	12.3298	12.3174	0.9982	13.6507	9.2438	8.8982
87	15.2188	15.1633	0.9964	17.6149	10.2112	9.7499

given by Eq. (3) for $\theta = 0$ is smaller than 1, due to the approximation procedure followed in order to determine Eq. (3).

Since an error seems to have crept into the above computations, so that the value of $m_a(\theta)$ at the horizon is equal to 36.2648 and, hence, results to be smaller by about 5% than the most realistic value given by precise calculations, Kasten and Young (1989) decided to recalculate the whole set of the optical mass for air, replacing the ARDC Model Atmosphere, 1959, with the ISO (International Standards Organization) Standard Atmosphere, 1972. This model is identical to the present Standard Atmospheres of ICAO (International Civil Aviation Organization) and WMO (World Meteorological Organization) up to a height of 32 km and presents lower temperatures and consequently higher values of air density than the ARDC Model Atmosphere, 1959, at all the stratospheric altitudes above 20 km. Moreover, this atmospheric model is defined with a height resolution twice as much as that of the previous model and gives air density values with one more decimal place. The values of the relative optical air mass $\mu_a(\theta)$ determined by Kasten and Young (1989) are also given in Table 1, together with the corresponding values of the ratio $\Gamma(\theta)$ between the values $\mu_a(\theta)$ calculated by Kasten and Young (1989) and those of $m_a(\theta)$ determined from Eq. (3). These values of $\Gamma(\theta)$ were found to range between 1.0005 and 1.0007 as θ increases from 0° to 82° and to decrease very slowly at higher angles to assume the values of 1.0000 at $\theta = 84^\circ$ and 0.9964 at $\theta = 87^\circ$.

2.2 *Kasten's Formula giving the Relative Optical Mass for Water Vapour*

It is well known that the dry air density decreases as a function of height describing an approximately exponential curve with a scale height of about 8 km (Penndorf, 1957). On the contrary, the vertical profiles of absolute humidity generally exhibit irregular shapes with large variations from a meteorological situation to another. On the basis of Eq. (2) and considering the most realistic distribution curves of absolute humidity as a function of height, Kasten (1966) proposed the following empirical formula,

$$m_w(\theta) = [\cos\theta + 0.0548\,(92.650 - \theta)^{-1.452}]^{-1}, \quad (4)$$

giving the relative optical mass for water vapour as a function of the apparent zenith angle θ of the sun for standard conditions of the atmosphere. The values of $m_w(\theta)$ obtained from Eq. (4) are given in Table 1 for thirty values of θ. It is interesting to notice that the value of $m_w(\theta)$ given by Eq. (4) at $\theta = 0^\circ$ is slightly smaller than 1, since Eq. (4) was determined through a best-fit procedure. The curve defined by Eq. (4) is compared in Fig. 2 to that of the relative optical air mass $m_a(\theta)$, showing that the relative optical

water-vapour mass presents slightly higher values than $m_a(\theta)$ at solar zenith angles smaller than 70° and increases more rapidly than $m_a(\theta)$ at higher zenith angles, up to the value of 17.615 at $\theta = 87°$. Such behaviour is plausibly due to the fact that a large fraction of precipitable water is contained within the lower part of the troposphere, while the vertical profile of air density exhibits a shape decreasing in an exponential manner with a scale height of about 8 km.

2.3 Young's Formula giving the Relative Optical Mass for Ozone

Atmospheric ozone strongly absorbs the incoming solar radiation at ultraviolet and visible wavelengths. The concentration of this triatomic molecule is relatively high in the stratospheric region between the 15 and 35 km altitudes and usually assumes very low values at tropospheric levels. The vertical profile of the ozone concentration generally exhibits a wide maximum, whose shape can vary widely as a function of both latitude and season. Thus, the mean monthly value of the vertical atmospheric content of ozone varies generally between 0.20 cm STP in the equatorial zone and no more than 0.40 cm STP at middle latitudes, although it can sometimes present large and rapid changes over a few days, in correspondence to tropopause folding episodes.

Using a very simple model of atmospheric ozone distribution, in which the ozone is assumed to be totally concentrated within a very thin layer situated at the altitude h, Young (1969) and Staehelin et al. (1995) proposed the following empirical formula,

$$m_o(\theta) = (R + h)[(R + h)^2 - R^2 \sin^2 \theta]^{-0.5} \qquad (5)$$

in order to calculate the relative optical ozone mass $m_o(\theta)$ at sea-level as a function of the solar zenith angle θ. Using this formula for a value of h equal to $h_o = 22$ km, chosen for a mid-latitude atmospheric model, we obtained the values of $m_o(\theta)$ given in Table 1. The corresponding dependence curve of $m_o(\theta)$ is shown in Fig. 2. The comparison of this curve with those of $m_a(\theta)$ and $m_w(\theta)$ clearly indicates that the relative optical ozone mass $m_o(\theta)$ varies as a function of θ in a very different manner from the other two optical mass functions within the range $\theta > 80°$.

2.4 Young's Formula giving the Relative Optical Mass for Nitrogen Dioxide

Solar radiations is also strongly absorbed by atmospheric nitrogen dioxide, since a wide band characterized by semicontinuous spectral features covers the wavelength range from 0.25 to nearly 0.60 μm. The atmospheric vertical content of NO_2 can vary largely with latitude and season, since the concentration of this molecule at stratospheric altitudes is closely related to the flux density of the incoming solar radiation in the ultraviolet and visible spectral range. Because of the intense photolytic processes occurring in the stratosphere, the vertical distribution curve of NO_2 concentration can exhibit large changes from day to night, at altitudes higher than 12 km. However, for standard mid-latitude conditions of the atmosphere, it presents at noon a wide maximum centred at about 18 km height (Brewer et al., 1973), so that the atmospheric vertical content C_n of NO_2 reaches its maximum during the diurnal period of maximum insolation and the following hours and presents the lowest values shortly before sunrise. Thus, the total volume content of these unstable molecules in the vertical atmospheric column of unit cross section can range between about $2\ 10^{-4}$ cm STP in the most remote regions of our planet and values higher than $8\ 10^{-3}$ cm STP in the most polluted urban areas (Brewer et al., 1973; Kulkarni, 1975).

In spite of the wide variability of the distribution characteristics of atmospheric NO_2, Eq. (5) has often been used to calculate the relative optical mass $m_n(\theta)$ for nitrogen dioxide as a function of the apparent solar zenith angle θ. The choice is justified by the fact that the greatest fraction of this atmospheric constituent is present in the stratospheric region between the altitudes of 15 and 30 km. Thus, we decided to use Eq. (5) to determine the dependence curve of $m_n(\theta)$ on θ by assuming that h is equal to the peak-altitude $h_n = 25$ km, according to the NO_2 concentration vertical profile adopted by Kneizys et al. (1988) in the atmospheric model "U.S. Standard Atmosphere 1976". These values of $m_n(\theta)$ are given in Table 1, while the curve of $m_n(\theta)$ as a function of angle θ is shown in Fig. 2. As can be seen, the dependence curves of $m_o(\theta)$ and $m_n(\theta)$ on angle θ are very similar since they were calculated

using Eq. (5) for values of h differing by 3 km only.

The four empirical formulas given in Eqs. (3) ÷ (5) for determining the air mass functions relative to dry air, water vapour, ozone and nitrogen dioxide were all determined for standard conditions of the atmosphere. However, the above remarks concerning the dependence of the optical mass functions on the thermal and composition characteristics of the atmosphere suggest that the functions $m_a(\theta)$, $m_w(\theta)$, $m_o(\theta)$ and $m_n(\theta)$ are expected to vary appreciably in all the cases where the vertical profiles of temperature, absolute humidity, ozone partial pressure and nitrogen dioxide partial pressure undergo considerable changes with latitude and season. All these aspects are examined in the following section.

3. Computational Programme and Atmospheric Models

In order to evaluate the extent to which the various relative optical mass functions can change as a consequence of the variations in the thermal and composition characteristics of the atmosphere, we decided to perform an extensive study based on calculations of the relative optical mass for air, water vapour, ozone and nitrogen dioxide at several values of θ and for the following nine atmospheric models, characterized by different meteorological conditions corresponding to various latitudes and seasons.

(1–6) The six models defined by McClatchey et al. (1972) and commonly known as

(1) the U. S. Standard Atmosphere 1976 (more briefly labelled US);

(2) the Mid-latitude Summer model (MS);

(3) the Mid-latitude Winter model (MW);

(4) the Subarctic Summer model (SS);

(5) the Subarctic Winter model (SW); and

(6) the Tropical model (TR).

Models (1) to (6) all exhibit the vertical profiles of air pressure, temperature, absolute humidity, ozone partial pressure and nitrogen dioxide mixing ratio defined by Kneizys et al. (1988) from sea-level to 100 km height. From these vertical profiles, we determined the values of the various meteorological and concentration parameters given in Table 2.

(7) The Indian Ocean model (IO), defined by Tomasi (1984) on the basis of a numerous set of radiosounding measurements taken in an oceanic area near the Seychelle Islands, within the altitude range from sea-level to 24 km. The model was completed with (i) the vertical profiles of air pressure, temperature and absolute humidity determined by Tomasi and Deserti (1988) in the height range from 24 to 100 km in accordance with those of model TR, and (ii) the vertical profiles of ozone partial pressure and nitrogen dioxide mixing ratio, as defined by Kneizys et al. (1988) in model TR.

(8) The July-75° N model (75 N), presenting average vertical profiles of air pressure, temperature, moisture parameters and volume concentrations of both ozone and nitrogen dioxide in the Arctic atmosphere during the summer period. These profiles are shown in Fig. 3.

The vertical profile of air pressure p was determined using (i) within the height range from sea-level to 30 km, the values given by the atmospheric model "75° N, July" (U.S. Standard Atmosphere Supplements, 1966) and (ii) within the altitude range 30 to 100 km, the values of p obtained through exponential interpolation in height between the value given at 30 km level by the atmospheric model "75° N, July" and that given at 118 km level by the atmospheric model "60° N, July" (U.S. Standard Atmosphere Supplements, 1966).

The vertical profile of temperature was defined (i) from sea-level to 30 km height, according to model "75° N, July", (ii) from 42 to 100 km height, according to model "60° N July", and (iii) from 30 to 42 km altitude, following a linear interpolation procedure in height.

The vertical profile of absolute humidity was determined (i) from sea-level to 10 km height, taking the values of moisture parameters given by the model "Arctic (75° N) Atmosphere, mean July" (Sissenwine, 1969), (ii) from 10 to 42 km level, following a linear interpolation procedure between the water vapour mixing ratio values proposed at the 75° N latitude by Schiff et al. (1985) at the pressure levels of 50 and 10 hPa, and (iii) from 42 to 100 km level, assuming a curve in close agreement with the data-set given by the Subarctic Summer model (SS) (McClatchey et al., 1972).

Table 2. *Values of Air Pressure p_o at Ground-level, Air Temperature T_o at Ground-level, Tropopause Height z_t, Air Temperature T_t at the Tropopause Level, Absolute Humidity q_o at Ground-level, Precipitable Water w, Altitude h_o of the Maximum Ozone Concentration, Vertical Atmospheric Content C_o of Ozone, Altitude h_n of the NO_2 Partial Pressure Maximum, and Vertical Atmospheric Content C_n of Nitrogen Dioxide*

Atmospheric model	p_o (hPa)	T_o (°K)	z_t (km)	T_t (°K)	q_o (g m^{-3})	w (g cm^{-2})	h_o (km)	C_o (cm STP)	h_n (km)	C_n (cm STP)
US	1013	288.2	12.0	216.7	5.9	1.42	22	0.345	25	$2.07\ 10^{-4}$
MS	1013	294.0	13.0	216.0	14.0	2.92	25	0.336	25	$2.22\ 10^{-4}$
MW	1018	272.2	19.0	215.2	3.5	0.85	21	0.378	25	$2.01\ 10^{-4}$
SS	1010	287.0	10.0	225.0	9.1	2.09	22	0.348	25	$2.19\ 10^{-4}$
SW	1013	257.1	9.0	217.2	1.2	0.42	20	0.376	25	$1.89\ 10^{-4}$
TR	1013	300.0	17.0	195.0	19.0	4.12	25	0.284	25	$2.14\ 10^{-4}$
IO	1013	300.6	17.5	189.3	22.4	5.11	25	0.286	25	$2.17\ 10^{-4}$
75N	1013	278.9	14.0	230.2	5.8	1.48	20	0.320	24	$1.96\ 10^{-4}$
75S	993	273.7	8.4	223.4	2.1	0.39	21	0.310	25	$2.26\ 10^{-4}$

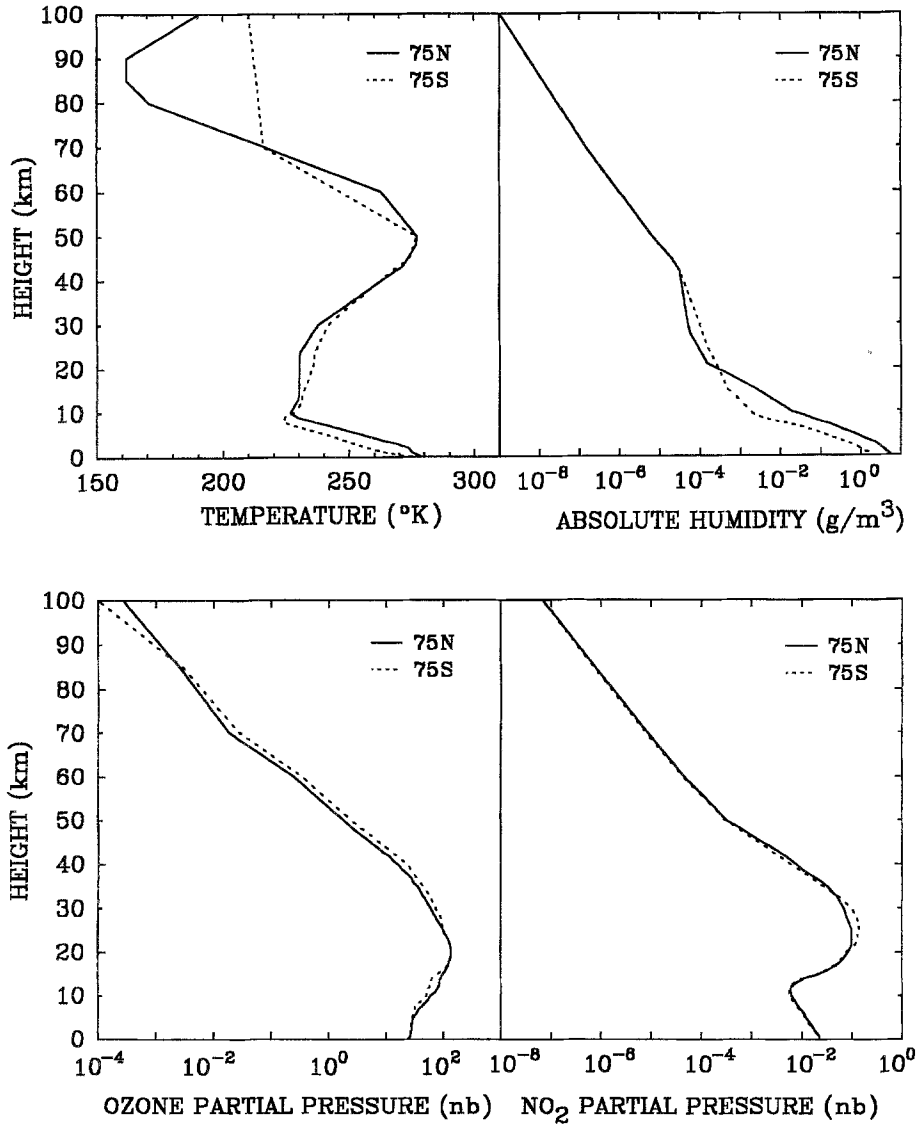

Fig. 3. Vertical profiles of air temperature, absolute humidity, ozone partial pressure and nitrogen dioxide partial pressure for the two atmospheric models 75 N and 75 S in the height range from sea-level to 100 km

Table 3. *Values of Ratio $f_a(\theta)$ for the Relative Optical Air Mass Obtained in Terms of Eq. (10) for thirty Values of the Apparent Solar Zenith Angle θ and the nine Atmospheric Models defined in Table 2*

θ(°)	Atmospherical Model								
	US	MS	MW	SS	SW	TR	IO	75N	75S
0	1.0005	1.0005	1.0005	1.0005	1.0005	1.0005	1.0005	1.0005	1.0005
10	1.0006	1.0006	1.0006	1.0006	1.0006	1.0006	1.0006	1.0006	1.0006
15	1.0006	1.0006	1.0006	1.0006	1.0006	1.0006	1.0006	1.0006	1.0006
20	1.0006	1.0006	1.0006	1.0006	1.0006	1.0006	1.0006	1.0006	1.0006
25	1.0006	1.0006	1.0006	1.0006	1.0006	1.0006	1.0006	1.0006	1.0006
30	1.0006	1.0006	1.0006	1.0006	1.0006	1.0005	1.0005	1.0006	1.0006
35	1.0006	1.0005	1.0006	1.0006	1.0006	1.0006	1.0005	1.0006	1.0006
40	1.0006	1.0006	1.0006	1.0006	1.0006	1.0005	1.0005	1.0006	1.0006
45	1.0006	1.0005	1.0006	1.0006	1.0007	1.0005	1.0005	1.0006	1.0006
50	1.0005	1.0004	1.0006	1.0005	1.0006	1.0004	1.0004	1.0005	1.0005
55	1.0004	1.0004	1.0005	1.0004	1.0006	1.0004	1.0003	1.0004	1.0006
60	1.0004	1.0004	1.0006	1.0004	1.0007	1.0003	1.0003	1.0005	1.0006
65	1.0005	1.0003	1.0007	1.0005	1.0008	1.0003	1.0002	1.0005	1.0007
68	1.0004	1.0002	1.0007	1.0004	1.0010	1.0002	1.0001	1.0005	1.0008
70	1.0005	1.0002	1.0008	1.0004	1.0011	1.0002	1.0001	1.0005	1.0008
72	1.0005	1.0002	1.0010	1.0005	1.0013	1.0002	1.0000	1.0006	1.0010
74	1.0006	1.0001	1.0011	1.0005	1.0016	1.0000	0.9999	1.0006	1.0011
75	1.0005	1.0000	1.0011	1.0005	1.0017	1.0000	0.9999	1.0007	1.0012
76	1.0006	1.0001	1.0012	1.0005	1.0019	1.0000	0.9998	1.0008	1.0014
77	1.0006	1.0000	1.0014	1.0005	1.0021	0.9998	0.9997	1.0008	1.0014
78	1.0006	0.9999	1.0015	1.0004	1.0024	0.9997	0.9996	1.0009	1.0016
79	1.0007	0.9997	1.0017	1.0004	1.0027	0.9996	0.9994	1.0009	1.0018
80	1.0006	0.9996	1.0019	1.0004	1.0031	0.9993	0.9992	1.0010	1.0020
81	1.0006	0.9994	1.0021	1.0003	1.0037	0.9990	0.9988	1.0011	1.0023
82	1.0006	0.9990	1.0023	1.0002	1.0043	0.9986	0.9984	1.0011	1.0026
83	1.0005	0.9985	1.0027	0.9999	1.0051	0.9979	0.9977	1.0011	1.0031
84	1.0001	0.9976	1.0030	0.9995	1.0062	0.9969	0.9966	1.0010	1.0035
85	0.9995	0.9962	1.0033	0.9987	1.0076	0.9952	0.9948	1.0008	1.0040
86	0.9984	0.9940	1.0037	0.9974	1.0095	0.9925	0.9920	1.0004	1.0047
87	0.9967	0.9907	1.0045	0.9956	1.0130	0.9883	0.9876	0.9998	1.0058

The vertical profile of ozone partial pressure was determined (i) in the height intervals from sea-level to 20 km and from 45 to 100 km, taking the values given by model SS (Kneizys et al., 1988), (ii) in the height range from 24 to 39 km, averaging at various heights the values given by model SS and those obtained by Solomon et al. (1985) and Bhartia et al. (1985), and (iii) in the two altitude intervals from 20 to 24 km and from 39 to 45 km, following a procedure of exponential interpolation of ozone partial pressure in height between the values fixed above. Subsequently, the vertical profile of ozone partial pressure characterized by a maximum at the 20 km height was normalized to give an atmospheric vertical content of ozone equal to 0.32 cm STP, according to London (1980).

The vertical profile of nitrogen dioxide partial pressure was determined as follows: (i) within the height intervals below 10 km and from 50 to 100 km, assuming the values given by model SS, (ii) in the altitude range from 10 to 45 km, averaging at various levels the values given by model SS and those found by Harries et al. (1985), and (iii) within the altitude range from 45 to 50 km, following an exponential interpolation procedure in height. This curve was found to present a marked peak at the 24 km height.

The most significant parameters of model 75 N are given in Table 2.

(9) The January-75° S model (75 S), determined on the basis of a large set of field measurements from which the vertical profiles of the four physical parameters shown in Fig. 3 were obtained. The vertical profiles of air pressure and temperature were determined in the altitude range from sea-level to 31 km averaging the mean vertical profiles found by Vitale and Tomasi (1994) from a set of 273 diurnal radiosounding measurements taken at the Terra Nova Bay station (164°07′ E; 74°42′ S) in Antarctica during the January period of five years. The vertical profile of air pressure was completed from 31 to 100 km level through an exponential interpolation procedure in height between the mean value given by Vitale and Tomasi (1994) at the 31 km height and that given by model "60° N, July" (U.S. Standard Atmosphere Supplements, 1966) at the 118 km level. The vertical profile of temperature was completed (i) within the altitude range from 42 to 100 km, assuming the values given by the atmospheric model SS (Kneizys et al., 1988), and (ii) in the altitude interval from 31 to 42 km, following a linear interpolation procedure in height. As can be seen in Table 3, the tropopause level was set at 8.4 km, with a temperature minimum of about 223° K.

The vertical profile of absolute humidity was determined (i) from sea-level to the 25 km height, averaging the moisture values measured by Vitale and Tomasi (1994) in January, (ii) from 25 to 42 km height, following a procedure of linear interpolation in height between the mixing ratio values found by Schiff et al. (1985) at the pressure levels of 50 and 10 hPa, and (iii) from 42 to 100 km level, assuming the moisture conditions of model SS. For this vertical curve of absolute humidity, the precipitable water was found to be equal to 0.39 g cm^{-2}. The estimate agrees very closely with the infrared hygrometer measurements of precipitable water carried out at the Terra Nova Bay station by Tomasi et al. (1990) during the January period of 1988 and 1989, giving values of this quantity ranging between 0.2 and 0.7 g cm^{-2}.

The vertical profile of ozone partial pressure was defined (i) in the height intervals from 0 to 10 km and from 40 to 100 km, adopting the values given by model SS, (ii) in the altitude range from 10 to 35 km, according to the values given by model SS and those found by Bhartia et al. (1985), Iwasaka and Kondoh (1987), Gernandt (1987) and Grose et al. (1989), and (iii) in the 35 to 40 km height interval, following an exponential interpolation procedure in height between the previous values. This average vertical distribution curve of ozone partial pressure presents its maximum value at the 21 km height and was subsequently normalized to give an atmospheric vertical content of ozone equal to 0.31 cm STP, as estimated by London (1980).

The vertical profile of NO_2 partial pressure was defined (i) in the height intervals from sea-level to 20 km and from 45 to 100 km, assuming the values given by model SS; (ii) from 27 to 34.5 km, averaging the values of mixing ratio found by Harries et al. (1985) and Callis and Natarajan (1986), and (iii) within the height intervals from 25 to 27 km and from 34.5 to 45 km, following an exponential interpolation procedure in height. This profile characterized by a marked peak situated at the 25 km height and provides an atmospheric vertical content of NO_2 equal to about 2.3 10^{-4} cm STP.

On the basis of these assumptions and calculations, we defined the vertical profiles of the meteorological and atmospheric composition parameters required to calculate the optical mass functions $m_a(\theta)$, $m_w(\theta)$, $m_o(\theta)$ and $m_n(\theta)$ for the nine atmospheric models described above. Among these models, those labelled IO and TR pertain to the 0° and 15° N latitudes, respectively. The mid-latitude models MS and MW refer to the two extreme seasons and pertain to the 45° N latitude, while model US can be used to represent the mean mid-latitude characteristics of the atmosphere during the intermediate seasons. Models SS and SW refer to the two extreme seasons at the 60° N latitude. Finally, models 75 N and 75 S represent the average atmospheric conditions in high-latitude areas during the maximum insolation period of the year.

Using the vertical profiles of the various atmospheric parameters given by the nine atmospheric models, we calculated the values of the four relative optical mass functions at several solar zenith angles θ ranging from 0° to 87°. For this purpose, we used the computer code LOWTRAN 7 prepared by Kneizys et al. (1988) for calculating, in accordance with Eq. (1), the geometrical length of any slant path described by

the solar radiation passing through the atmosphere and the total optical mass of each atmospheric constituent distributed along the sun-path. Precise evaluations of the optical mass pertinent to both the vertical and slant paths of the atmosphere can be correctly obtained only if the effects due to the earth's curvature and air refraction are taken into account with a good accuracy together with all variations in temperature, absolute humidity, ozone partial pressure and NO_2 partial pressure occurring over small distances in height. Therefore, we decided to divide each atmospheric model given in Table 2 into the following ninety-six layers:

(i) sixteen layers of 0.25 km depth from sea-level to 4 km height;
(ii) sixty-four layers of 0.5 km depth from 4 to 36 km;
(iii) ten sub-layers of 1.0 km depth from 36 to 46 km;
(iv) two sub-layers of 2.0 km depth from 46 to 50 km;
(v) two sub-layers of 10 km depth from 50 to 70 km;
(vi) two sub-layers of 15 km depth from 70 to 100 km.

Within the layers, the temperature was assumed to vary linearly as a function of height, while the other parameters (air pressure, air density, air refractive index, absolute humidity and partial pressure of both ozone and NO_2) were assumed to vary exponentially as a function of height. Such assumptions were made for all the nine atmospheric models and for all the layers listed above. Using the computer code LOWTRAN 7, we calculated the values of optical mass m relative to the slant path in terms of Eq. (1) and of optical mass m_z relative to the vertical direction for the nine atmospheric models and the thirty values of the apparent solar zenith angle θ listed in Table 1. More precisely, we calculated parameters m and m_z relative to the air at wavelength $\lambda = 0.55\,\mu m$, parameters m and m_z for water vapour at wavelength $\lambda = 0.935\,\mu m$, parameters m and m_z for ozone at wavelength $\lambda = 0.32\,\mu m$, and parameters m and m_z for nitrogen dioxide at wavelength $\lambda = 0.39\,\mu m$, that is at wavelengths situated in the middle parts of the spectral intervals where the various atmospheric constituents extinguish most strongly the solar radiation.

From these calculations, we determined the values of the relative optical mass functions $M_a(\theta)$, $M_w(\theta)$, $M_o(\theta)$ and $M_n(\theta)$ as ratios between the values of optical mass m and the corresponding values of m_z, as obtained for each of the four atmospheric constituents considered above. The mass functions $M_a(\theta)$, $M_w(\theta)$, $M_o(\theta)$ and $M_n(\theta)$ were found to vary differently as a function of θ, mainly as a result of variations in the vertical profiles of the air temperature and the molecular concentrations of the minor atmospheric constituents.

4. Dependence Features of the Relative Optical Air Mass on Latitude, Season and Temperature Inversion Conditions

Following the above procedure, we calculated the values of relative optical air mass $M_a(\theta)$ for all the nine atmospheric models listed in Table 2 and for a great number of values of θ ranging from 0° to 87°. All values of the apparent solar zenith angle θ were calculated at the ground level by taking into account for each atmospheric model all the refraction effects produced by the atmosphere during the passage of the incoming solar radiation. Thereupon, in order to evaluate the variations in $M_a(\theta)$ due to modifications in the latitudinal and seasonal conditions of the atmosphere, we calculated the ratios $f_a(\theta) = M_a(\theta)/m_a(\theta)$ for all the values of $M_a(\theta)$ found above and the corresponding values of $m_a(\theta)$ given in Table 1. The values of ratio $f_a(\theta)$ obtained for all the nine atmospheric models are given in Table 3 for thirty values of θ in the 0° to 87° range. Each ratio $f_a(\theta)$ gives a measure of the relative difference between the present evaluations of the relative optical air mass and those given by Kasten (1966). Therefore, this set of values offers an exhaustive picture of the variations in the relative optical air mass which can be caused by changes in the thermal characteristics of the atmosphere due to latitude and season. The dependence curves of $f_a(\theta)$ on θ in the upper range of θ are shown in the left part of Fig. 4. The curve found for the US model maintains values close to the unity from 0° to 84° and falls appreciably below the unity only for $\theta > 85°$. In the atmospheric models characterized by cold

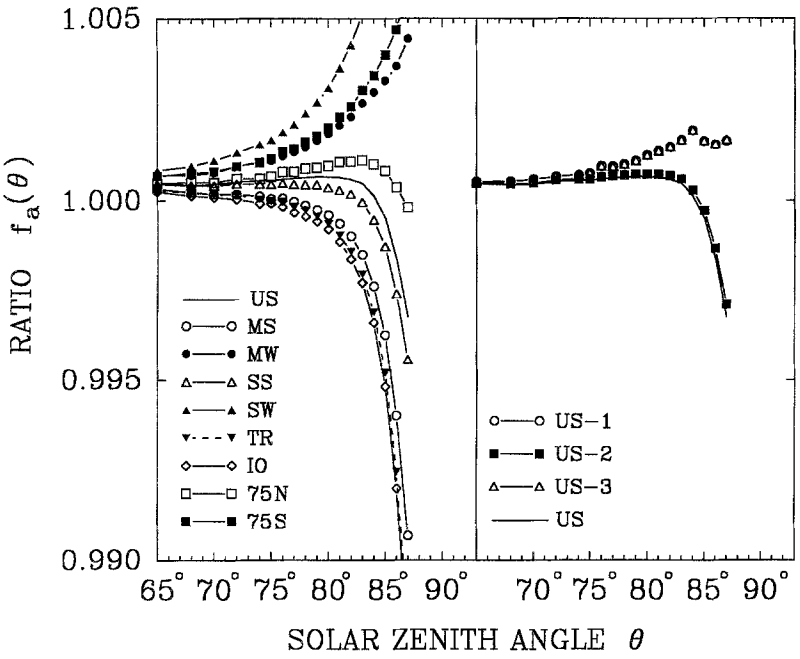

Fig. 4. Ratio $f_a(\theta)$ as a function of the apparent solar zenith angle θ in the range from 65° to 87° for twelve atmospheric models: on the left, the curves pertinent to the nine models US, MS, MW, SS, SW, TR, IO, 75N and 75S, all listed in Table 2; on the right, the four curves relative to models US-1, US-2, US-3 and US (shown for comparison)

and relatively dry air conditions, such as models MW, 75S and SW, parameter $f_a(\theta)$ increases slightly as a function of θ, reaching values of between 1.005 and 1.013 at $\theta = 87°$. In atmospheric models presenting relatively moderate temperature conditions, such as models 75N, SS and US, ratio $f_a(\theta)$ assumes very stable values varying by less than 0.1% throughout the whole range $\theta < 85°$ and by less than 1% as θ increases from 85° to 87°. In atmospheric models characterized by warm air conditions, such as models MS, TR and IO, $f_a(\theta)$ decreases by less than 0.1% throughout the range of θ from 0° to 80° and falls rapidly beyond 80°, until decreasing by 1% or more at $\theta = 87°$. These results show that the values given by the Kasten (1966) formula as well as those determined by Kasten and Young (1989) are very realistic and require only weak corrections in extreme cases of temperature conditions.

Since the air refraction effects are closely related to the vertical gradient of the air temperature, the presence of strong thermal inversions within the ground layer of the atmosphere could cause significant modifications in the relative optical air mass. In order to verify the consistency of this hypothesis and at the same time evaluate the variability range of the relative optical air mass associated with strong inversions of the atmospheric temperature, we calculated the values of $M_a(\theta)$ for the three atmospheric models US-1, US-2, and US-3, presenting the vertical profiles of temperature shown in Fig. 5 within the height range from 0 to 3 km and the same profile of model US at higher altitudes. These three models represent very extreme conditions of temperature in the low troposphere, since model US-1 is characterized by strong cooling conditions near the ground, model US-2 exhibits a superadiabatic gradient of air temperature in the ground layer of 1 km depth and a strong temperature inversion between the 1 and 2 km levels and model US-3 presents two strong temperature inversion layers between the altitudes of 0 and 0.5 km and those of 1 and 2 km.

We calculated the values of $M_a(\theta)$ for these three models and divided them by the corresponding values of $m_a(\theta)$ in Table 1 obtaining the three curves of $f_a(\theta)$ shown in the right hand part of Fig. 4. The results show that ratios $f_a(\theta)$ relative to models US-1 and US-3 increase by only a few thousandths as a function of θ, throughout the range of θ from 65° to 87°, while ratio $f_a(\theta)$ relative to model US-2 decreases by no more than $4\ 10^{-3}$ as θ increases from 80° to 87°. This indicates that the relative optical air mass is subject to increase very slightly also in cases of very intense cooling processes causing strong

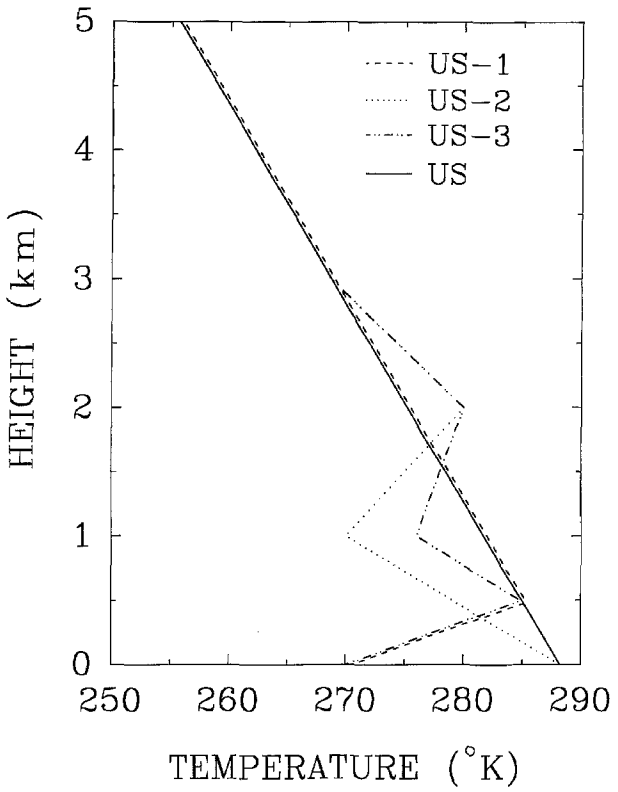

Fig. 5. Vertical profiles of air temperature adopted in models US-1, US-2, US-3 and US, within the height range from sea-level to 5 km

thermal inversion layers near the ground. Moreover, this function is estimated to decrease by no more than 1% for values of θ close to 87° also in extreme cases where the ground heating produces superadiabatic conditions of the temperature gradient throughout the ground-layer.

5. Dependence Features of the Relative Optical Water Vapour Mass on Latitude, Season and Atmospheric Moisture Conditions

For all the values of relative optical water vapour mass $M_w(\theta)$ found for the nine atmospheric models described in Table 2, we determined the ratios $f_w(\theta) = M_w(\theta)/m_w(\theta)$, where $m_w(\theta)$ is calculated according to Eq. (4). These values of $f_w(\theta)$ are given in Table 4, while the corresponding dependence curves of $f_w(\theta)$ on angle θ are shown in the left part of Fig. 6. All these curves present values of $f_w(\theta)$ very close to the unity in the range of $\theta < 80°$ and then increase more steeply until exceeding the unity by more than 1% for $\theta > 86°$. These results clearly indicate that the Kasten formula in Eq. (4) can be reliably used to calculate the relative optical mass for water vapour at high zenith angles θ for all the atmospheric conditions which do not differ considerably from those described by standard models. However, examining the various characteristics of the atmospheric models in Table 2, it appears reasonable to explain some differences in the evaluations of $f_w(\theta)$ in terms of the different vertical distribution curves of absolute humidity adopted in the various models. The discrepancies between the values of $M_w(\theta)$ from one atmospheric model to another are probably due to the greater or lesser percentages of precipitable water present within the low troposphere, where the most significant refraction effects take place. In fact, considering the ground-layer of 2 km depth, we found relatively low values of $f_w(\theta)$ for models 75 N, SW, US and IO, which contain percentages of precipitable water w within this ground-layer of 58%, 54%, 60% and 61%, respectively. On the contrary, high values of $f_w(\theta)$ were obtained for models 75 S, MS, TR and MW, which present percentages of w equal to 69%, 65%, 65% and 60%, respectively. These considerations suggest that the values of ratio $f_w(\theta)$ should increase in an almost proportional manner as the percentage of w contained in the ground-layer of the atmosphere becomes gradually greater. In order to verify the validity of this statement, we decided to calculate the values of $M_w(\theta)$ and $f_w(\theta)$ for three other atmospheric models, all obtained by strongly modifying the vertical distribution curve of relative humidity given in model US:

(1) model US-A, which differs from model US in the vertical profile of relative humidity since this parameter was assumed to increase from 30% at sea-level to 52% at the 2 km level and to present higher values than those of model US from 2 to 8 km height, so as to give a value of precipitable water $w = 1.41\ \mathrm{g\,cm^{-2}}$ and a fraction of w equal to 49% in the ground-layer of 2 km depth;

(2) model US-B, which presents the same values of relative humidity as in model US-A from sea-level to 2 km altitude and the same values of model US from 2 to 100 km level, giving $w = 1.26\ \mathrm{g\,cm^{-2}}$ and a percentage of w in the ground-layer of 2 km depth equal to 55%;

Table 4. *Values of Ratio $f_w(\theta)$ for the Relative Optical Water Vapour Mass Obtained in Terms of Eq. (11) for thirty Values of the Apparent Solar Zenith Angle θ and the nine Atmospheric Models Defined in Table 2*

$\theta(°)$	Atmospheric model								
	US	MS	MW	SS	SW	TR	IO	75N	75S
0	1.0001	1.0001	1.0001	1.0001	1.0001	1.0001	1.0001	1.0001	1.0001
10	1.0001	1.0001	1.0001	1.0001	1.0001	1.0002	1.0002	1.0001	1.0002
15	1.0002	1.0002	1.0002	1.0002	1.0002	1.0002	1.0003	1.0002	1.0003
20	1.0002	1.0002	1.0002	1.0001	1.0001	1.0001	1.0002	1.0002	1.0002
25	1.0002	1.0002	1.0002	1.0003	1.0002	1.0002	1.0002	1.0001	1.0002
30	1.0000	0.9999	1.0000	1.0000	1.0000	0.9999	1.0000	1.0000	1.0000
35	1.0000	1.0000	1.0000	1.0000	1.0000	0.9999	1.0000	1.0000	1.0001
40	1.0000	0.9999	1.0000	1.0000	1.0000	1.0000	1.0000	0.9999	1.0000
45	1.0002	0.9999	1.0001	1.0000	1.0000	1.0000	1.0001	1.0001	1.0002
50	0.9998	0.9996	0.9998	0.9997	0.9999	0.9997	0.9997	0.9997	0.9998
55	0.9997	0.9995	0.9998	0.9996	0.9998	0.9995	0.9997	0.9997	0.9997
60	0.9997	0.9996	0.9998	0.9997	1.0000	0.9996	0.9998	0.9997	0.9999
65	1.0000	0.9996	0.9999	0.9999	0.9998	0.9998	0.9999	0.9998	1.0002
68	0.9998	0.9996	1.0000	0.9998	0.9998	0.9997	0.9997	0.9996	0.9999
70	0.9997	0.9998	0.9999	0.9997	1.0000	0.9996	0.9999	0.9999	1.0000
72	1.0000	0.9999	1.0001	1.0000	1.0000	1.0000	0.9999	1.0000	1.0006
74	0.9999	0.9999	1.0001	0.9999	1.0000	0.9998	1.0000	1.0000	1.0003
75	1.0001	1.0000	1.0000	1.0001	1.0000	0.9998	1.0000	1.0001	1.0005
76	1.0003	1.0004	1.0005	1.0003	1.0003	1.0001	1.0002	1.0001	1.0009
77	1.0000	1.0000	1.0002	1.0000	1.0003	1.0003	1.0000	0.9999	1.0008
78	1.0003	1.0004	1.0006	1.0004	1.0005	1.0005	1.0001	1.0004	1.0014
79	1.0004	1.0005	1.0007	1.0005	1.0005	1.0005	1.0004	1.0003	1.0016
80	1.0007	1.0008	1.0009	1.0008	1.0006	1.0007	1.0005	1.0005	1.0019
81	1.0010	1.0014	1.0015	1.0011	1.0010	1.0013	1.0010	1.0009	1.0027
82	1.0012	1.0017	1.0017	1.0013	1.0012	0.0018	1.0013	1.0012	1.0033
83	1.0021	1.0029	1.0026	1.0023	1.0021	1.0029	1.0019	1.0023	1.0051
84	1.0027	1.0042	1.0037	1.0030	1.0029	1.0038	1.0028	1.0030	1.0066
85	1.0042	1.0062	1.0056	1.0045	1.0042	1.0058	1.0042	1.0043	1.0093
86	1.0063	1.0094	1.0084	1.0068	1.0060	1.0090	1.0066	1.0069	1.0144
87	1.0101	1.0154	1.0132	1.0109	1.0092	1.0143	1.0102	1.0106	1.0227

(3) model US-C, which presents the same values of relative humidity as in model US from sea-level to 2 km height and from 8 to 100 km, and the same values of relative humidity taken in model US-A within the height range from 2 to 8 km, so as to give $w = 1.57\,\mathrm{g\,cm^{-2}}$ and a percentage of w in the ground-layer equal to 54%.

The values of $f_w(\theta)$ found for these three models are compared in the right part of Fig. 6 to the dependence curve referring to model US. As can be noticed, these results fully confirm the above hypothesis about the existence of a proportionality trend between $f_w(\theta)$ and the percentage content of the water vapour mass in the ground-layer of the atmosphere. In fact, the values of $f_w(\theta)$ found for model US-A (49%) decrease below the unity as θ increases, while those obtained for models US-B (55%) and US-C (54%) both tend to increase by a few thousandths as θ increases from 70° to 87°, although at appreciably slower rates than for model US (60%). On the basis of these finding, we can state that, in general, the values of $f_w(\theta)$ corresponding to high values of θ assume higher values for thermodynamic conditions of the atmosphere for which the percentage of precipitable water in the lower tropospheric layer is high. In fact, in our evaluations, $f_w(87°)$ was found to assume a value lower than 1 for model US-A (49%), values ranging between 1.00 and 1.01 for models US-B, US-C, 75N, SW and US (with percentages of w ranging between 54% and 60%), values varying between 1.01 and 1.016 for models SS, IO, MW, MS and TR (all with percentages ranging from

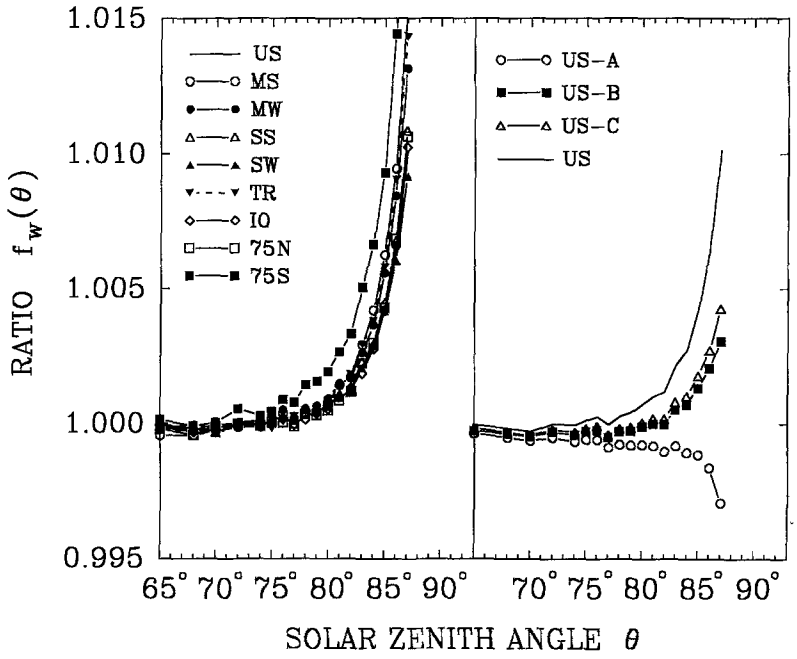

Fig. 6. Ratio $f_w(\theta)$ as a function of the apparent solar zenith angle θ in the range from 65° to 87° for twelve atmospheric models: on the left, the curves pertinent to the nine models US, MS, MW, SS, SW, TR, IO, 75N and 75S; on the right, the four curves relative to models US-A, US-B, US-C, and US (shown for comparison)

60% to 65%) and a value higher than 1.02 for model 75S (69%).

6. Dependence Features of the Relative Optical Ozone Mass on Latitude and Season

The values of the relative optical ozone mass $M_o(\theta)$ were calculated using the computer code LOWTRAN 7 for the nine atmospheric models in Table 2. From these values, we determined the corresponding values of ratio $f_o(\theta) = M_o(\theta)/m_o(\theta)$, using the values of $m_o(\theta)$ obtained in terms of Eq. (5), for a value of $h = 22$ km. The values of ratio $f_o(\theta)$ found for thirty values of θ ranging from 0° to 87° are given in Table 5, while the dependence curves of $f_o(\theta)$ on θ are shown in the left part of Fig. 7. The results indicate very clearly that the relative optical ozone mass corresponding to high values of θ increases more rapidly as a function of θ in atmospheres where the vertical content of ozone assumes rather high values and the ozone partial pressure peak is situated at lower altitudes (i. e., passing from the equatorial zone to the high-latitude regions). In fact, the lowest values of $f_o(\theta)$ were found for models TR and IO, while intermediate values of $f_o(\theta)$ were found for models US, MS and SS, and the highest values of $f_o(\theta)$ (exceeding the unity by more than 8% at $\theta = 87°$) were obtained for models MW, SW, 75N and 75S. In order to verify the validity of these remarks about the existence of a close relationship between ratio $f_o(\theta)$ and the peak level of ozone concentration, we calculated the values of $M_o(\theta)$ and $f_o(\theta)$ for two atmospheric models obtained from model US by simply modifying the shape of the vertical profile of ozone partial pressure, as follows:

(1) model US-a, in which the vertical profile of ozone partial pressure was assumed to be the one shown in the left part of Fig. 8, with the peak situated at an altitude of 25 km and the total ozone content C_o taken to be equal to 0.345 cm STP, as in model US;

(2) model US-b, in which the total ozone content is the same as that of models US and US-a, being the vertical profile of ozone partial pressure taken to have the peak at an altitude of 18 km, as shown in the left part of Fig. 8.

The corresponding dependence curves of $f_o(\theta)$ on θ are compared in the right part of Fig. 7 with the curve of $f_o(\theta)$ found for the original version of model US. The curve of $f_o(\theta)$ found for model US-a presents considerably lower values than the unity at all the values of θ ranging between 75° and 87°, while that pertinent to model US-b presents appreciably higher values of $f_o(\theta)$ than those found for model US. This test confirms that function $M_o(\theta)$ relative to high values of θ should

Table 5. *Values of Ratio $f_o(\theta)$ for the Relative Optical Ozone Mass Obtained in Terms of Eq. (12) for thirty Values of the Apparent Solar Zenith Angle and the nine Atmospheric Models Defined in Table 2*

θ(°)	Atmospheric model								
	US	MS	MW	SS	SW	TR	IO	75N	75S
0	1.0000	1.0000	1.0000	1.0000	1.0000	1.0000	1.0000	1.0000	1.0000
10	1.0000	1.0000	1.0000	1.0000	1.0000	1.0000	1.0000	1.0000	1.0000
15	1.0000	1.0000	1.0000	1.0000	1.0000	1.0000	1.0000	1.0001	1.0000
20	1.0000	1.0000	1.0001	1.0000	1.0001	1.0000	1.0000	1.0001	1.0001
25	1.0000	1.0000	1.0001	1.0001	1.0001	0.9999	0.9999	1.0001	1.0001
30	1.0000	1.0000	1.0001	1.0001	1.0002	0.9999	0.9999	1.0002	1.0001
35	1.0001	1.0000	1.0002	1.0001	1.0003	0.9999	0.9999	1.0003	1.0002
40	1.0001	1.0000	1.0003	1.0002	1.0004	0.9998	0.9998	1.0003	1.0002
45	1.0002	1.0001	1.0004	1.0003	1.0005	0.9998	0.9997	1.0005	1.0004
50	1.0002	1.0001	1.0006	1.0003	1.0007	0.9996	0.9996	1.0006	1.0005
55	1.0003	1.0001	1.0008	1.0005	1.0011	0.9994	0.9994	1.0010	1.0007
60	1.0005	1.0002	1.0012	1.0007	1.0016	0.9992	0.9992	1.0014	1.0010
65	1.0008	1.0004	1.0019	1.0011	1.0024	0.9988	0.9988	1.0022	1.0016
68	1.0011	1.0006	1.0025	1.0015	1.0032	0.9985	0.9987	1.0030	1.0021
70	1.0014	1.0007	1.0031	1.0019	1.0040	0.9982	0.9982	1.0037	1.0026
72	1.0018	1.0009	1.0039	1.0024	1.0050	0.9978	0.9978	1.0046	1.0033
74	1.0023	1.0012	1.0050	1.0032	1.0063	0.9973	0.9973	1.0059	1.0043
75	1.0027	1.0015	1.0057	1.0036	1.0073	0.9970	0.9970	1.0068	1.0049
76	1.0031	1.0017	1.0066	1.0043	1.0083	0.9967	0.9966	1.0078	1.0058
77	1.0037	1.0021	1.0077	1.0050	1.0096	0.9963	0.9963	1.0091	1.0067
78	1.0044	1.0026	1.0091	1.0059	1.0113	0.9959	0.9958	1.0107	1.0079
79	1.0053	1.0033	1.0108	1.0071	1.0134	0.9954	0.9954	1.0127	1.0095
80	1.0066	1.0042	1.0130	1.0087	1.0161	0.9948	0.9948	1.0153	1.0116
81	1.0083	1.0055	1.0160	1.0109	1.0196	0.9944	0.9943	1.0187	1.0143
82	1.0107	1.0074	1.0200	1.0139	1.0241	0.9939	0.9940	1.0234	1.0181
83	1.0142	1.0102	1.0255	1.0182	1.0305	0.9938	0.9937	1.0297	1.0235
84	1.0192	1.0147	1.0333	1.0245	1.0394	0.9941	0.9941	1.0388	1.0312
85	1.0269	1.0218	1.0446	1.0338	1.0521	0.9958	0.9958	1.0520	1.0428
86	1.0389	1.0333	1.0614	1.0485	1.0702	1.0003	1.0002	1.0716	1.0607
87	1.0575	1.0525	1.0866	1.0709	1.0968	1.0104	1.0100	1.1011	1.0885

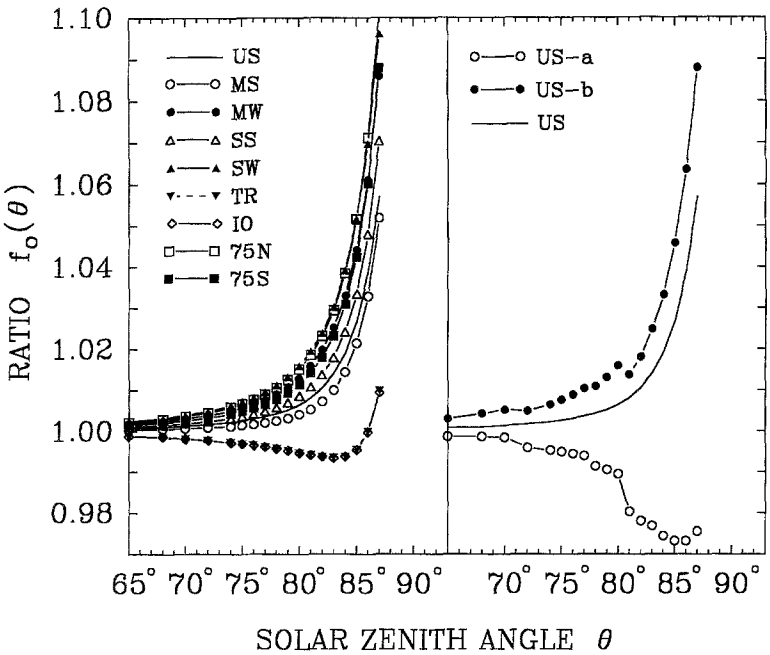

Fig. 7. Ratio $f_o(\theta)$ as a function of the apparent solar zenith angle θ in the range from 65° to 87° for eleven atmospheric models: on the left, the curves pertinent to the nine models US, MS, MW, SS, SW, TR, IO, 75N and 75S; on the right, the three curves relative to models US-a, US-b and US (shown for comparison)

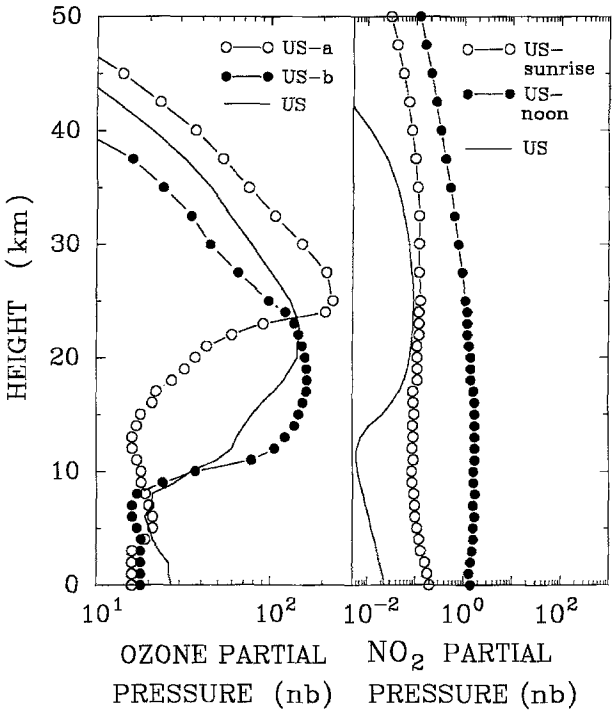

Fig. 8. On the left: vertical profiles of ozone partial pressure (measured in nbar), relative to atmospheric models US, US-a and US-b, in the height range from sea-level to 50 km. On the right: vertical profiles of NO_2 partial pressure adopted in models US, US-sunrise and US-noon within the same altitude range, according to Brewer et al. (1973)

assume appreciably lower values than those obtained for mid-latitude standard conditions, in all the cases where the peak of ozone concentration is located at relatively high altitudes. On the contrary, in the cases where the vertical distribution curves of ozone concentration exhibit their peak at low altitudes, function $M_o(\theta)$ should assume higher values, so as to give values of $f_o(\theta)$ exceeding that relative to the standard atmosphere by at least 3% at $\theta = 85°$.

7. Dependence Features of Relative Optical Nitrogen Dioxide Mass on Latitude and Season

The values of relative optical nitrogen dioxide $M_n(\theta)$ were calculated using the code LOWTRAN 7 for the nine models in Table 2. Using these values and those of $m_n(\theta)$ calculated in terms of Eq. (5) for the peak altitude $h = h_n = 25$ km, we determined the corresponding values of ratio $f_n(\theta) = M_n(\theta)/m_n(\theta)$ for the thirty selected values of θ from 0° to 87°. These values of $f_n(\theta)$ are given in Table 6, while their angular dependence curves are shown in the left part of Fig. 9. The results very clearly show that the ratio $f_n(\theta)$ assumes slightly greater values than the unity at low solar zenith angles and increases gradually as a function of θ to exceed the value of 1.03 at $\theta = 85°$ and to reach values higher than 1.06 at $\theta = 87°$ for all the models. In particular, ratio $f_n(\theta)$ was found to exceed the value of 1.08 at $\theta = 87°$ for the two models SW and 75N, which are both characterized by very low values of the vertical content of NO_2, as can be noticed in Table 2.

More generally, the angular dependence curves of $f_n(\theta)$ shown in the left part of Fig. 9 appear to be very similar also at high values of θ. This behaviour is presumably due to the fact that the vertical content of NO_2 varies only between 1.9 10^{-4} and 2.3 10^{-4} cm STP for the nine atmospheric models listed in Table 2 and the peak altitude of NO_2 concentration is around 25 km for all these models. However, it appears plausible to state that ratio $f_n(\theta)$ varies appreciably with the height of the concentration peak and the shape of the vertical profile of NO_2 concentration, as a result of similar effects to those suggested above for the ozone function $f_o(\theta)$. In particular, ratio $f_n(\theta)$ should assume higher values in all the cases where the total atmospheric content of NO_2 increases considerably. By way of verification, we calculated the functions $M_n(\theta)$ and $f_n(\theta)$ for the two atmospheric models US-sunrise and US-noon, which have been derived from model US by only changing the vertical profile of NO_2 partial pressure adopted by Kneizys et al. (1988), in such a way as to obtain two very different values of the total atmospheric content C_n of NO_2. As shown in the right part of Fig. 8, model US-sunrise exhibits the vertical profile of NO_2 partial pressure determined by Brewer et al. (1973) at sunrise, giving C_n equal to 5.75 10^{-4} cm STP (which is almost three times as high as that of model US). Model US-noon presents the vertical profile of NO_2 partial pressure defined by Brewer et al. (1973) at noon and, hence, is characterized by values of NO_2 volume concentration considerably higher than those found at sunrise at all the stratospheric levels. Consequently, C_n is equal to 5.81 to 10^{-3} cm STP, that is about twenty-eight times greater than that of model US. The

Table 6. *Values of Ratio $f_n(\theta)$ for the Relative Optical Nitrogen Dioxide Mass Obtained in Terms of Eq. (13) for Thirty Values of the Apparent Solar Zenith Angle θ and the nine Atmospheric Models Defined in Table 2*

θ(°)	Atmospheric model								
	US	MS	MW	SS	SW	TR	IO	75N	75S
0	1.0000	1.0000	1.0000	1.0000	1.0000	1.0000	1.0000	1.0000	1.0000
10	1.0001	1.0001	1.0001	1.0002	1.0000	1.0001	1.0001	1.0001	1.0000
15	1.0000	1.0001	1.0002	1.0001	1.0002	1.0001	1.0000	1.0001	1.0000
20	1.0003	1.0003	1.0002	1.0003	1.0003	1.0002	1.0002	1.0003	1.0002
25	1.0000	1.0001	1.0001	1.0000	0.9999	1.0000	1.0001	1.0000	1.0000
30	1.0004	1.0004	1.0004	1.0005	1.0003	1.0004	1.0004	1.0004	1.0003
35	1.0003	1.0003	1.0004	1.0004	1.0004	1.0003	1.0004	1.0003	1.0004
40	1.0006	1.0005	1.0005	1.0005	1.0006	1.0005	1.0005	1.0006	1.0006
45	1.0005	1.0006	1.0007	1.0006	1.0006	1.0007	1.0007	1.0007	1.0007
50	1.0008	1.0008	1.0009	1.0009	1.0009	1.0009	1.0010	1.0010	1.0008
55	1.0012	1.0012	1.0012	1.0011	1.0012	1.0013	1.0011	1.0013	1.0012
60	1.0015	1.0015	1.0017	1.0015	1.0017	1.0016	1.0016	1.0018	1.0016
65	1.0017	1.0015	1.0018	1.0015	1.0020	1.0017	1.0017	1.0021	1.0019
68	1.0023	1.0021	1.0021	1.0021	1.0027	1.0024	1.0023	1.0029	1.0025
70	1.0029	1.0026	1.0030	1.0026	1.0033	1.0029	1.0028	1.0036	1.0031
72	1.0033	1.0029	1.0035	1.0028	1.0040	1.0033	1.0033	1.0043	1.0037
74	1.0042	1.0038	1.0046	1.0037	1.0051	1.0042	1.0042	1.0055	1.0047
75	1.0048	1.0044	1.0053	1.0042	1.0058	1.0049	1.0048	1.0063	1.0054
76	1.0056	1.0050	1.0062	1.0050	1.0067	1.0057	1.0056	1.0073	1.0063
77	1.0065	1.0060	1.0071	1.0059	1.0078	1.0066	1.0066	1.0085	1.0072
78	1.0074	1.0067	1.0081	1.0065	1.0090	1.0075	1.0075	1.0096	1.0083
79	1.0088	1.0080	1.0098	1.0079	1.0107	1.0090	1.0088	1.0115	1.0099
80	1.0106	1.0097	1.0118	1.0096	1.0129	1.0108	1.0108	1.0137	1.0118
81	1.0119	1.0107	1.0132	1.0103	1.0146	1.0120	1.0119	1.0155	1.0134
82	1.0150	1.0135	1.0167	1.0131	1.0183	1.0151	1.0150	1.0194	1.0168
83	1.0195	1.0178	1.0216	1.0173	1.0236	1.0198	1.0196	1.0248	1.0215
84	1.0257	1.0234	1.0283	1.0231	1.0308	1.0259	1.0257	1.0323	1.0279
85	1.0349	1.0320	1.0381	1.0315	1.0415	1.0350	1.0347	1.0429	1.0369
86	1.0485	1.0447	1.0526	1.0441	1.0571	1.0485	1.0480	1.0585	1.0505
87	1.0690	1.0637	1.0745	1.0632	1.0808	1.0686	1.0678	1.0816	1.0703

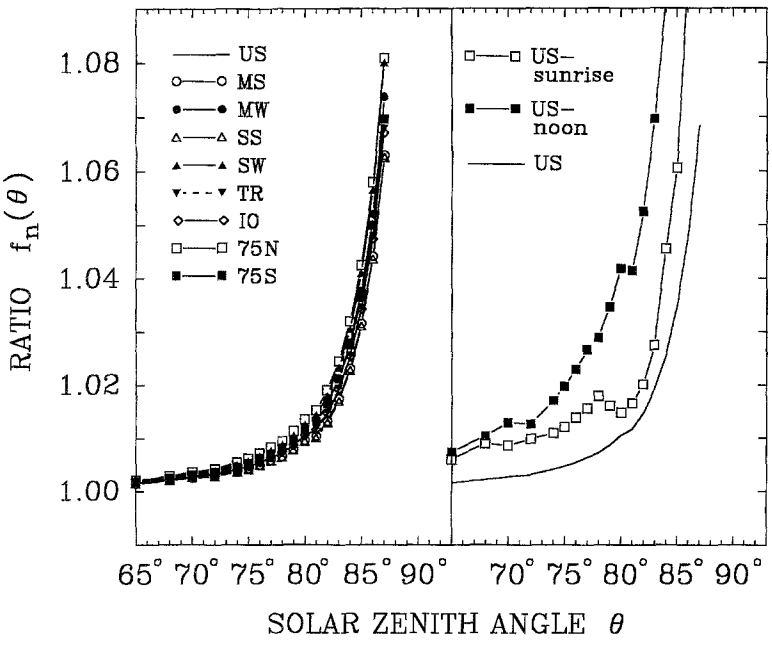

Fig. 9. Ratio $f_n(\theta)$ as a function of the apparent solar zenith angle θ in the range from 65° to 87° for eleven atmospheric models: on the left, the curves pertinent to the nine models US, MS, MW, SS, SW, TR, IO, 75N and 75S; on the right, the three curves relative to models US-sunrise, US-noon and US (shown for comparison)

comparison of these two curves of $f_n(\theta)$ with that of model US is shown in the right part of Fig. 9. These results indicate that the daily variations in the vertical profile of NO_2 volume concentration causing a large increase in the total atmospheric content of NO_2 can produce a very marked increase in the relative optical mass for nitrogen dioxide, also at relatively low values of θ, showing an increment of ratio $f_n(\theta)$ greater than 15% at $\theta = 87°$. Therefore, the day-to-night changes in C_n as well as the modifications in the shape of the vertical profile of NO_2 partial pressure (due to the daily and/or seasonal changes in the incoming flux of solar radiation) are expected to cause appreciable changes in the dependence curves of relative optical nitrogen dioxide mass on the zenith angle θ, within the range $\theta > 75°$.

8. Conclusions

The present study of the dependence features of the relative optical mass functions for air, water vapour, ozone and nitrogen dioxide on the apparent solar zenith angle θ, as found for different latitudinal and seasonal conditions of the atmosphere, clearly indicates that:

(1) the angular dependence curve of relative optical air mass $M_a(\theta)$ can vary appreciably at high values of θ, as a consequence of latitudinal, seasonal and daily changes in the thermal characteristics of the atmosphere. However, the evaluations given by the Kasten (1966) formula in Eq. (3) and those provided by Kasten and Young (1989) allow one to obtain reliable estimates of the relative optical air mass for conditions not far from those of the standard atmosphere, at all values of θ. At high values of θ, the air mass function $M_a(\theta)$ was found to assume slightly higher values than those found by Kasten (1966) for atmospheric models characterized by cold and dry air conditions and appreciably lower values than Kasten's (1966) evaluations for mid- and low-latitude models of the atmosphere, characterized by warm air conditions. Thermal inversions near the ground or at upper heights are expected to cause only changes of a few thousandths in the relative optical air mass, also at $\theta = 87°$. The values of ratio $f_a(\theta)$ given in Table 3 and the results shown in Fig. 4 can be usefully employed in order to obtain reliable estimates of $M_a(\theta)$ for different atmospheric conditions.

(2) The angular dependence curve of relative optical mass for water vapour $M_w(\theta)$ is appreciably influenced by latitudinal and seasonal variations in the moisture conditions of the atmosphere only for angles $\theta > 80°$. The Kasten (1966) formula in Eq. (4) was found to give reliable estimates of $M_w(\theta)$ for all the atmospheric conditions and throughout the whole range $\theta < 80°$, while it furnishes appreciably underestimated values at higher angles. In fact, the present results clearly indicate that $M_w(\theta)$ is subject to significant changes at values of $\theta > 80°$, when modifications in the vertical distribution curve of absolute humidity take place, due to meteorological events or seasonal changes in the thermodynamic structure of the atmosphere. In particular, our evaluations of ratio $f_w(\theta)$ show that $M_w(\theta)$ assumes higher values than those obtained from the Kasten (1966) formula in the cases where the percentage of precipitable water in the ground-layer of 2 km depth is greater than 54%, to an extent increasing with the percentage. Our calculations indicate that the value of $M_w(87°)$ can increase by about 2% as the percentage of w in the first 2 km of the atmosphere increases from about 50% to nearly 70%. In order to determine realistic values of $M_w(\theta)$ in the upper range of θ, the present calculations of function $f_w(\theta)$ given in Table 4 and shown in Fig. 6 can be used appropriately.

(3) The angular dependence curve of relative optical mass for ozone $M_o(\theta)$ is strongly related to the latitudinal and seasonal variations in the vertical distribution curve of ozone concentration. The Young (1969) formula in Eq. (5), based on the choice of a fixed value of the concentration peak altitude $h_o = 22$ km, does not take into account the changes in the ozonosphere structure due to latitude and season. The present results indicate with full clarity that this formula relative to sea-level measurements provides reliable results for values of θ smaller than 70° but does not furnish realistic estimates for higher solar zenith angles. Our calculations show that $M_o(\theta)$ assumes lower values than those given by Eq. (5) for low-latitudes models of the atmosphere and presents gradually higher values than those given by Eq. (5) for mid- and high-latitude models. Correct evaluations of $M_o(\theta)$ can be found using

the values of ratio $f_o(\theta)$ given in Table 5 and those shown in Fig. 7, since all these calculations were performed for atmospheric models in which the shape of the vertical profile of ozone partial pressure and the peak level of this profile have been changed taking into account both latitudinal and seasonal effects.

(4) The angular dependence curve of relative optical mass for nitrogen dioxide $M_n(\theta)$ was found to be significantly influenced by the latitudinal, seasonal and daily variations in the vertical distribution curve of NO_2 concentration. The formula in Eq. (5), used for a value of the concentration peak altitude $h = h_n = 25$ km, provides reliable evaluations of this optical parameter for all the atmospheric models considered here and at values of θ smaller than 70°. The results obtained at higher angles indicate that $M_n(\theta)$ can increase by several percents as a consequence of an increment in the total atmospheric content of this triatomic molecule, due to the daily effects produced by solar radiation or other dynamical and chemical effects related to latitude and season. Using the values of ratio $f_n(\theta)$ given in Table 6 and the results shown in Fig. 9, reliable values of $M_n(\theta)$ can be determined by taking into account the variations in both the vertical distribution curve and the atmospheric content of this minor constituent of the atmosphere.

Acknowledgements

This research was performed in the framework of the project "CLEARCOLUMN-ACE2", funded by the European Commission Programme "Environment and Climate".

References

Bhartia, P. K., Fleig, A., Froidevaux, L., Heath, D., Hilsenrath, E., Logan, J. A., McCormick, P., Megie, G., Nagatani, R., Russell, J. M. III, Thomas, R. J., 1985: Oxygen Species. In : *Atmospheric Ozone 1985,* WMO, Global Ozone Research and Monitoring Project, Report No. 16, Vol. II, 401–440.

Brewer, A. W., 1973: A replacement for the Dobson spectrophotometer?. *Pure Appl. Geophys.*, **106**, 919–927.

Brewer, A. W., McElroy, C. T., Kerr, J. B., 1973: Nitrogen dioxide concentrations in the atmosphere. *Nature,* **246**, 129–133.

Callis, L. B., Natarajan, M., 1986: The Antarctic ozone minimum: relationship to odd nitrogen, odd chlorine, the final warming, and the 11-year solar cycle. *J. Geophys. Res.,* **91**, 10771–10796.

Dobson, G. M. B., 1931: A photoelectric spectrophotometer for measuring atmospheric ozone. *Proc. Phys. Soc.,* **43**, 324–328.

Gernandt, H., 1987: The vertical ozone distribution above the GDR-Research Base, Antarctica in 1985. *Geophys. Res. Letters,* **14**, 84–86.

Grose, W. L., Jones, R. L., McCormick, M. P., Molina, M. J., O'Neil, A., Poole, L. R., Shine, K. P., Solomon, S., Plumb, R. A., Pope, V., 1989: Polar Ozone. In: *Scientific Assessment of Stratospheric Ozone 1989,* WMO, Global Ozone Research and Monitoring Project, Report No. 20, Vol. I, 1–161.

Harries, J, E., Brasseur, G., Coffey, M. T., Fisher, H., Gille, J., Jones, R., Lousnard, N., McCormick, M. P., Noxon, J., Owens, A. J., Pyle, J., Ridley, B. A., Roscoe, H., Schmeltekopf, A. L., Solomon, S., Sze, N. D., 1985: Nitrogen Species. In: *Atmospheric Ozone 1985,* WMO, Global Ozone Research and Monitoring Project, Report No. 16, Vol. II, 497–604.

ISO Standard Atmosphere, 1972: International Organization for Standardization, *Standard Atmosphere,* International Standard ISO 2533.

Iqbal, M., 1983: *An Introduction to Solar Radiation.* Toronto, Academic Press, 390 pp.

Iwasaka, Y., Kondoh, K., 1987: Depletion of Antarctic ozone: height of ozone loss region and its temporal changes. *Geophys. Res. Letters,* **14**, 87–90.

Kasten, F., 1966: A new table and approximation formula for the relative optical air mass. *Arch. Met. Geophys. Biokl., Ser. B,* **14(2)**, 206–223.

Kasten, F., Young, A. T., 1989: Revised optical air mass tables and approximation formula. *Appl. Opt.,* **28**, 4735–4738.

Kneizys, F. X., Shettle, E. P., Abreu, L. W., Chetwynd, J. H., Anderson, G.P., Gallery, W. O., Selby, J. E. A., Clough, S. A., 1988: *User Guide to LOWTRAN 7,* Environ. Res. Papers, No. 1010, AFGL-TR-88–0177. Air Force Geophysics Laboratory, Hanscom, Massachusetts, 137 pp.

Kulkarni, R. N., 1975: Measurements of NO_2 using the Dobson spectrophotometer. *J. Atmos. Sci.,* **32**, 1641–1643.

London, J., 1980: Radiative energy sources and sinks in the stratosphere and mesosphere. In: Aikin, A. C., (ed.) *Proceedings of the NATO Advanced Study Institute on Atmospheric Ozone: Its Variations and Human Influences.* Washington D. C.: U. S. Department of Transportation, 703–721.

McClatchey, R. A., Fenn, R. W., Selby, J. E. A., Volz, F. E., Garing, J. S., 1972: *Optical Properties of the Atmosphere (Third Edition),* Environ. Res. Papers, No. 411, AFCRL-72–0497, Air Force Geophysics Laboratory, L. G. Hanscom Field, Massachusetts, 108 pp.

Minzner, R. A., Champion, K. S. W., Pond, H. L., 1959: *The ARDC Model Atmosphere, 1959.* (Air Force Surveys in Geophysics, No. 115) Massachusetts: Air Force Cambridge Research Center.

Nakajima, T., Tonna, G., Rao, R., Boi, P., Kaufman, Y., Holben, B., 1996: Use of sky brightness measurements from ground for remote sensing of particulate polydispersions. *Appl. Opt.,* **35**, 2672–2686.

Penndorf, R., 1957: Tables of the refractive index of the standard air and the Rayleigh scattering coefficient for the

spectral region between 0.2 and 20.0 μm and their application to the atmospheric optics. *J. Opt. Soc. Am.,* **47**, 176–182.

Schiff, H. J., Burnet, C., Carli, B., DeMore, W. B., deZafra, R., Evans, W. F. J., Guthrie, P. D., Hampson, R. F., Heaps, W., Jones, R., Kley, D., Prather, M., Russell, J. M. III, Schmidt, U., Traub, W. A., Watson, R. T., 1985: Hydrogen Species. In: *Atmospheric Ozone 1985,* WMO, Global Ozone Research and Monitoring Project, Report No. 16, Vol. II, 441–496.

Shaw, G, E., 1976: Error analysis of multi-wavelength sun photometry. *Pure Appl. Geophys.,* **114**, 1–14.

Sissenwine, N., 1969: Standard and Supplemental Atmospheres. In: Ferrell Rex, D., (ed.) *World Survey of Climatology – Climate of the Free Atmosphere,* Vol. 4. Amsterdam: Elsevier, pp. 5–44.

Solomon, S., Garcia, R. R., Stordal, F., 1985: Transport processes and ozone perturbation. *J. Geophys. Res.,* **90**, 12981–12990.

Staehelin, J., Schill, H., Högger, B., Viatte, P., Levrat, G., Gamma, A., 1995: Total ozone observation by sun photometry at Arosa, Switzerland. *Opt. Engin.,* **34**, 1977–1986.

Thomason, L. W., Herman, B. M., Reagan, J. A., 1983: The effect of atmospheric attenuators with structured vertical distributions on air mass determinations and Langley plot analyses. *J. Atmos. Sci.,* **40**, 1851–1854.

Tomasi, C., Prodi, F., Sentimenti, M., Cesari, G., 1983: Multiwavelength sun-photometers for accurate measurements of atmospheric extinction in the visible and near-IR spectral range. *Appl. Opt.,* **22**, 622–630.

Tomasi, C., 1984: Vertical distribution features of atmospheric water vapor in the Mediterranean, Red Sea and Indian Ocean. *J. Geophys. Res.,* **89**, 2563–2566.

Tomasi, C., Deserti, M., 1988: *Vertical Distribution Models of Water Vapour for Radiative Transfer Calculations in the Atmosphere.* Techn. Paper No. 1, FISBAT-TP-88/1, C. N. R., Bologna, Italy, 196 pp.

Tomasi, C., Vitale, V., Tagliazucca, M., Gasperoni, L., 1990: Infrared hygrometry measurements at Terra Nova Bay. *SIF Conference Proceedings,* **27**, 187–200.

U. S. Standard Atmosphere Supplements, 1966: edited by Environmental Science Services Administration, National Aeronautics and Space Administration and United States Air Force, Washington D. C., U. S. Government Printing Office, 11–145.

Vitale, V., Tomasi, C., 1994: A correction procedure for determining the vertical profile of absolute humidity from the radiosounding measurements taken in the Antarctic atmosphere. *SIF Conference Proceedings,* **45**, 87–118.

Volz, F. E., 1974: Economical multispectral sun photometer for measurements of aerosol extinction from 0.44 μm to 1.6 μm and precipitable water. *Appl. Opt.,* **13**, 1732–1733.

Young, A. T., 1969: High-resolution photometry of a thin planetary atmosphere. *Icarus,* **11**, 1–23.

Author's address: Claudio Tomasi and Vito Vitale, Istituto FISBAT-CNR, Via Gobetti 101, I-40129 Bologna, Italy; Lucia Vincenza De Santis, Istituto ISIATA-CNR, Strada per Arnesano 1, I-73100 Lecce, Italy.